ORIGINAL PAPER

Structure and lithium mobility of Li_4Pt_3Si

**Tim Dinges · Rolf-Dieter Hoffmann · Leo van Wüllen ·
Paul Henry · Hellmut Eckert · Rainer Pöttgen**

Abstract The lithium-rich silicide Li_4Pt_3Si was synthesised from the elements by high-temperature synthesis in a sealed niobium ampoule. Its structure was refined on the basis of single-crystal X-ray diffraction data: $R32$, $a=693.7(2)$, $c=1627.1(4)$ pm, $wR2=0.0762$, 525 F^2 values and 21 variables. The striking structural motifs of the Li_4Pt_3Si structure are silicon atoms with a slightly distorted trigonal prismatic platinum coordination with short Si–Pt distances (238–246 pm). Always two trigonal prisms are condensed via a common Pt_3 triangle, and these double units built up a three-dimensional network by condensation via common corners. The channels left by this prismatic network are filled by two crystallographically independent lithium sites in a 3:1 ratio. The single crystal X-ray data were fully confirmed by neutron powder diffraction and ^7Li magic-angle spinning (MAS)–nuclear magnetic resonance (NMR) results. The two distinct lithium sites are well differentiated by their ^7Li isotropic chemical shift and nuclear electric quadrupolar interaction parameters. MAS-NMR spectra reveal signal coalescence effects above 300 K, indicating chemical exchange between the lithium sites on the millisecond timescale. The spectra can be simulated with a simple two-site exchange model. From the resulting temperature-dependent correlation times, an activation energy of 50 kJ/mol is extracted.

Keywords Intermetallic lithium compounds · Crystal chemistry · Solid-state NMR · Lithium mobility

T. Dinges · R.-D. Hoffmann · R. Pöttgen (✉)
Institut für Anorganische und Analytische Chemie,
Universität Münster,
Corrensstrasse 30,
48149 Münster, Germany
e-mail: pottgen@uni-muenster.de

L. van Wüllen · H. Eckert
Institut für Physikalische Chemie, Universität Münster,
Corrensstrasse 30,
48149 Münster, Germany

H. Eckert
e-mail: eckerth@uni-muenster.de

P. Henry
Institut für Komplexe Magnetische Materialien,
Helmholtz-Zentrum für Materialien und Energie,
Lise-Meitner-Campus,
Hahn-Meitner-Platz 1,
14109 Berlin, Germany
e-mail: paul.henry@helmholtz-berlin.de

Introduction

Among the many ternary Li–T–X (T = transition metal; X = tetrelide) systems, those with the $5d$ transition metals have so far only scarcely been investigated. The ternary compounds in these systems are good candidates for battery anode materials [1, 2]; however, noble metals containing ones are certainly not applicable for density as well as for financial reasons. Nevertheless, the $Li_xT_yX_z$ compounds exhibit interesting crystal chemistry and also substantial lithium mobility. Thus, they are interesting model systems for anode materials.

Fully characterised compounds with the $5d$ transition metals only exist for the stannide series. A structurally very interesting example concerns the solid solution $Li_{3-x}Pt_2Sn_{3+x}$ [3] which originally derives from the binary fluorite type stannide $PtSn_2$. First, one observes lithium occupancy of the octahedral voids left by the platinum atoms and subsequently part of the tin sites is substituted by lithium. At the line composition $Li_3Pt_2Sn_3$, one observes a well-ordered superstructure with a $2a×2b×2c$ supercell.

The iridium-based stannide LiIrSn$_4$ [4] crystallises with an ordered variant of the PdGa$_5$ type. The iridium atoms show square-antiprismatic tin coordination. These prisms are condensed to blocks which are separated by lithium atoms in a slightly stuffed square-prismatic coordination. On the nuclear magnetic resonance (NMR) timescale (data up to 450 K), the lithium atoms show no long-range diffusion [5]. Time-dependent electrochemical polarisation techniques, i.e. coulometric titration, chronopotentiometry, chronoamperometry and cyclic voltammetry, were used to study the kinetics of lithium ion diffusion in this stannide [6]. The range of homogeneity ($Li_{1+\Delta\delta}IrSn_4$, $-0.091 \leq \delta \leq +0.012$) without any structural change in the host structure and the chemical diffusion coefficient ($\sim 10^{-7}$–10^{-9} cm^2 s^{-1}) point out that LiIrSn$_4$ is a potential electrode material for rechargeable lithium batteries.

The tetragonal gold compound Li$_2$AuSn$_2$ consists of a rigid three-dimensional $[AuSn_2]^{\delta-}$ network in which the lithium ions fill channels within the a and b directions. ^{7}Li solid-state NMR data show the onset of substantial line narrowing around 300 K and an activation energy of lithium motion of 27 kJ mol^{-1}. Galvanostatic intermittent titration technique and potentiometric intermittent titration technique techniques were employed to study the kinetics of lithium ion diffusion. The chemical diffusion coefficient of lithium was determined as a function of the lithium non-stoichiometry x with respect to Li$_{2+x}$AuSn$_2$ having a maximum value $D_{Li-max}=1.5\times^{-6}$ cm^2 s^{-1} at the lowest lithium content of $x=0$ at 25 °C [7].

In continuation of our systematic phase analytical studies of the Li–T–X systems ([8, 9] and references therein), we obtained the new lithium-rich silicide Li$_4$Pt$_3$Si. The structural data and the ^{7}Li solid-state NMR spectroscopic investigation are reported herein. A preliminary account on the Li$_4$Pt$_3$Si structure was presented at a conference [10].

Experimental techniques

Syntheses

Starting materials for the preparation of the Li$_4$Pt$_3$Si sample were lithium rods (Merck, >99%), platinum sheet (Heraeus, >99.9%) and silicon lumps (Wacker, >99.9%). The lithium rods were cut into smaller pieces under dry paraffin oil and subsequently washed with n-hexane. The lithium pieces were kept in Schlenk tubes under argon prior to the reaction. Argon was purified with titanium sponge (900 K), silica gel and molecular sieves. The lithium pieces were mixed with the cut platinum sheet and the silicon lumps in the ideal 4:3:1 atomic ratio under flowing argon, and then arc-welded [11] in a niobium ampoule under an argon pressure of about 700 mbar. The niobium tube was

subsequently enclosed in an evacuated silica tube for oxidation protection. The sample was heated to 1,373 K within 5 h and kept at this temperature for another 2 h. Thereafter, the tube was cooled to 1,023 K at a rate of 1 K/min. After 1 week of annealing, the sample was quenched in ice water. The sample is not stable in air and was therefore kept in an argon-filled Schlenk tube. Single crystals exhibit metallic lustre, whilst powders are dark grey.

EDX analyses

Selected Li$_4$Pt$_3$Si single crystals and also the bulk phase were studied by energy-dispersive analyses of X-rays (EDX) using a Leica 420i scanning electron microscope with Pt and SiO$_2$ as standards. The semiquantitative analyses were always close to the 3:1 platinum/silicon ratio. No impurity elements heavier than sodium (detection limit of the instrument) have been detected.

X-ray powder diffraction

The Li$_4$Pt$_3$Si sample was characterised through a Guinier powder pattern (Cu Kα_1 radiation, α-quartz: $a=491.30$ and $c=540.46$ pm as internal standard). The Guinier camera was equipped with an imaging plate technique (Fujifilm, BAS-READER 1800). The hexagonal lattice parameters (Table 1) were obtained through a least-squares routine. The correct indexing was ensured through a comparison of the experimental pattern with a calculated one [12].

Single-crystal X-ray data

Irregularly shaped crystal fragments of Li$_4$Pt$_3$Si were selected from the annealed sample by mechanical fragmentation. The moisture-sensitive crystals were glued to the tip of small quartz Mark capillaries and then sealed in Mark capillaries with a slightly larger diameter. Subsequently, the crystals were investigated by Laue photographs on a Buerger camera (white molybdenum radiation, image plate technique, Fujifilm, BAS-1800) in order to check their quality for intensity data collection. The data set was collected at room temperature using an IPDS II diffractometer (graphite monochromatized Mo Kα radiation, oscillation mode). A numerical absorption correction was applied to the data set. Details on the crystallographic data measurements are given in Table 1.

Neutron powder diffraction

Neutron diffraction data of Li$_4$Pt$_3$Si were collected on the fine-resolution powder diffractometer E9 at the BENSC, Berlin Neutron Scattering Center, Helmholtz-Zentrum für Materialien und Energie, Berlin. A cylindrical aluminium

Table 1 Crystal data and structure refinement for Li$_4$Pt$_3$Si

Empirical formula	Li$_4$Pt$_3$Si
Formula weight	641.12 g/mol
Unit cell dimensions (powder data)	a=693.7(2) pm
	c=1627.1(4) pm
	V=0.6781 nm^3
Space group	R32 (155)
Formula units per cell	Z=6
Calculated density	9.42 g/cm^3
Crystal size	$40\times40\times60\,\mu m^3$
Transmission ratio (max/min)	0.472:0.120
Absorption coefficient	92.7 mm^{-1}
F(000)	1,560
Detector distance	80 mm
Exposure time	14 min
ω range; increment	0–180°, 1.0°
Integration parameters A, B, EMS	14.0, 2.5, 0.022
θ range for data collection	3°–32°
Range in hkl	±10, ±10, ±24
Total no. of reflections	2,729
Independent reflections	525 (R_{int}=0.0468)
Reflections with $I\geq2\sigma(I)$	457 (R_{sigma}=0.0433)
Data/parameters	525/21
Goodness-of-fit on F^2	0.96
Final R indices [$I\geq2\sigma(I)$]	$R1$=0.0337; $wR2$=0.0748
R indices (all data)	$R1$=0.0407; $wR2$=0.0762
Flack parameter	−0.02(8)
Extinction coefficient	0.00069(7)
Largest diff. peak and hole	3.92 and −3.28 e/Å^3

container was filled with ~5 g of the fine ground sample in an argon box and closed with a copper seal. The collection of intensity data (λ=179.7 pm) was carried out for 20 h within a 2θ range from 4° to 158° at room temperature. Rietveld analysis of the neutron data was carried out using Jana2006 [13].

Solid-state NMR spectroscopy

^{7}Li NMR spectra were measured on a Bruker DSX 500 spectrometer, interfaced to an 11.7-T magnet. Data were acquired with 45° pulses of 4.5-μs length and relaxation delays of 10 s. Static spectra in the temperature range 290 K<T<440 K and magic-angle spinning experiments (spinning rate = 10 kHz) in the temperature range 290 K<T <460 K were carried out using a commercial 4-mm magic angle spinning (MAS)–NMR probe. Chemical shifts are reported relative to a 1 M LiCl aqueous solution. Spectra were deconvoluted into Gauss–Lorentz functions using the DMfit programme [14].

Results and discussion

Structure determination and refinement

Analyses of the diffractometer data set clearly revealed a rhombohedral lattice and no further extinctions, leading to the space groups $R\overline{3}m$, $R3m$, $R32$ $R\overline{3}$, and $R3$, of which the non-centrosymmetric group $R32$ was found to be correct during the structure refinements. The starting atomic parameters of the platinum and silicon atoms were deduced from an interpretation of direct methods with SHELXS-97 [15], and the lithium sites were located from subsequent difference Fourier synthesis. Subsequently, the structure was refined using SHELXL–97 (full-matrix least-squares on F^2) [16] with anisotropic atomic displacement parameters for the platinum and silicon and isotropic displacement parameters for the lithium atoms. As a check for the correct composition, the occupancy parameters of the platinum and silicon sites were refined in a separate series of least-squares cycles. They were all fully occupied within two standard deviations. Free refinement of the lithium occupancies was not reliable. In the final cycles, the ideal occupancy was assumed again. The final difference electron density synthesis was flat. The highest residual peak was

Table 2 Atomic coordinates and isotropic displacement parameters (pm^2) for Li$_4$Pt$_3$Si

U_{eq} is defined as one third of the trace of the orthogonalized U_{ij} tensor. The positional parameters obtained by a Rietveld refinement of neutron powder data are listed for comparison in italics

Atom	Wyckoff position	x	y	z	U_{eq}/U_{iso}
Li1	6c	0	0	0.725(3)	107(97)
		0	*0*	*0.726(1)*	
Li2	18f	0.363(6)	0.932(7)	0.087(2)	212(71)
		0.356(2)	*0.931(2)*	*0.0826(9)*	
Pt1	9e	0.6070(2)	0	1/2	108(2)
		0.6088(4)	*0*	*1/2*	
Pt2	9d	0.7389(1)	0	0	106(2)
		0.7386(4)	*0*	*0*	
Si	6c	0	0	0.1020(5)	105(15)
		0	*0*	*0.1031(5)*	

Table 3 Interatomic distances (pm) for Li₄Pt₃Si (calculated with the powder lattice parameters; standard deviations are given in parenthesis)

Li1:	3	Li2	255(4)	Pt1:	2	Si	238.1(4)
	3	Pt1	277(3)		2	Li2	257(4)
	3	Pt2	277(2)		2	Pt2	274.12(7)
	1	Si	281(5)		2	Li1	277(3)
	3	Li2	294(5)		2	Li2	280(4)
Li2:	1	Li1	255(4)		2	Li2	288(4)
	1	Pt1	257(4)	Pt2:	2	Si	245.6(5)
	1	Pt2	260(4)		2	Li2	260(4)
	1	Li2	263(8)		2	Pt1	275.12(7)
	1	Pt2	279(4)		2	Li1	277(2)
	1	Si	279(4)		2	Li2	279(4)
	1	Pt1	280(4)		2	Li2	305(4)
	1	Pt1	288(4)		2	Pt2	313.7(2)
	1	Li2	293(8)	Si:	3	Pt1	238.1(4)
	1	Li1	294(5)		3	Pt2	245.6(5)
	2	Li2	303(7)		3	Li2	279(4)
	1	Pt2	305(4)		1	Li1	281(5)

All distances of the first coordination spheres are listed

close to the platinum atoms and most likely resulted from an incomplete absorption correction. Refinement of the correct absolute structure was ensured through a calculation of the Flack parameter [17, 18]. The results of the structure refinement are summarised in Table 1. The atomic coordinates and the interatomic distances are listed in Tables 2 and 3. Further information on the structure refinement is available from Fachinformationszentrum

Fig. 1 Crystal structure of Li₄Pt₃Si; view approximately along the x-axis. Lithium and platinum atoms are drawn as *light grey* and *black filled circles*, respectively. The network of condensed SiPt₆ trigonal prisms is emphasised
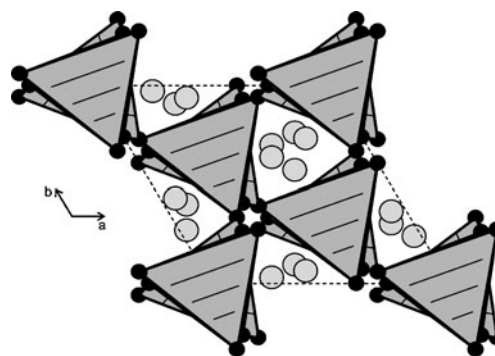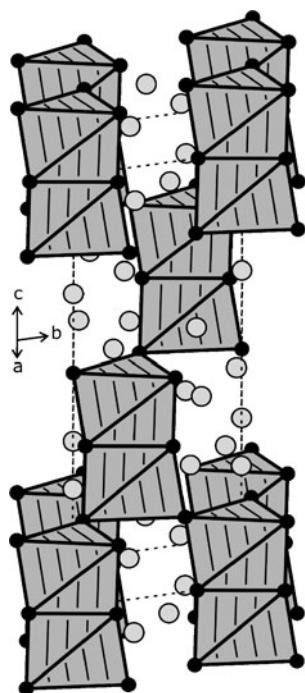
Fig. 2 Projection of the Li₄Pt₃Si structure along the z-axis. Lithium and platinum atoms are drawn as *light grey* and *black filled circles*, respectively. The network of condensed SiPt₆ trigonal prisms is emphasised

Karlsruhe, D-76344 Eggenstein-Leopoldshafen (Germany), by quoting Registry no. CSD–421984.

The complementary neutron diffraction experiment provided a good confirmation of the refined single-crystal data and let to a reliable refinement of the two lithium positions (full occupancy) in the structure: space group R32, R_p=6.71, R_{wp}=8.93, R(all)=3.82, Rw(all) 4.82. For comparison, the refined positional parameters are listed in Table 2.

Crystal chemistry

The non-centrosymmetric structure of Li₄Pt₃Si contains two crystallographically independent platinum sites and one silicon site. The silicon atoms are coordinated to six platinum atoms (3×Pt1 and 3×Pt2) in a slightly distorted trigonal prismatic arrangement. Two such prisms are condensed via the Pt2 triangles to double units and the latter further condensed via common Pt1 corners, leading to the three-dimensional network presented in Fig. 1. The ABC stacking sequence of the Pt₉Si₂ units nicely reflects
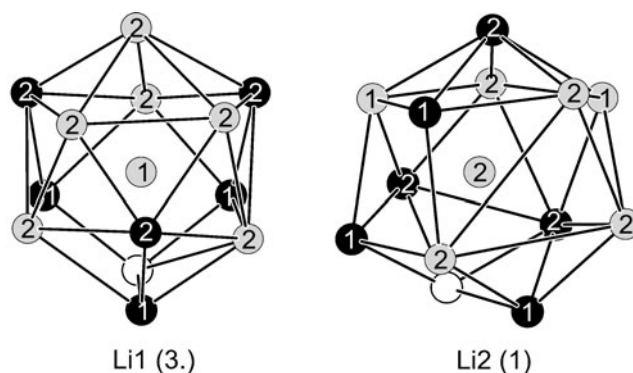
Fig. 3 Coordination polyhedra of the lithium atoms in the Li₄Pt₃Si structure. Lithium, platinum and silicon atoms are drawn as *light grey*, *black filled* and *open circles*, respectively. The site symmetries are indicated
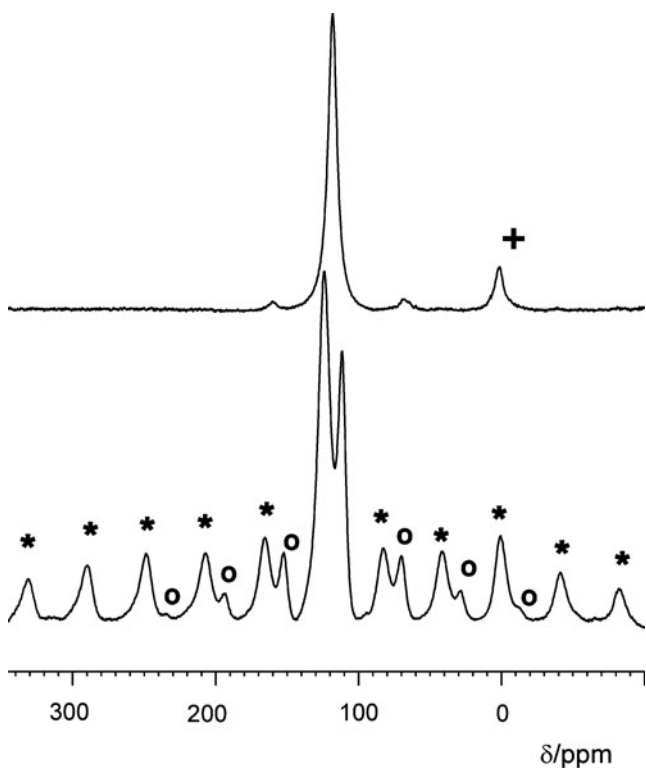
Fig. 4 ^{7}Li MAS-NMR spectra of Li_4Pt_3Si at 300 K (*bottom*) and 470 K (*top*). The feature marked by the *plus sign* is attributed to an oxidic impurity. Spinning sideband manifolds for the two sites are marked by *asterisks*
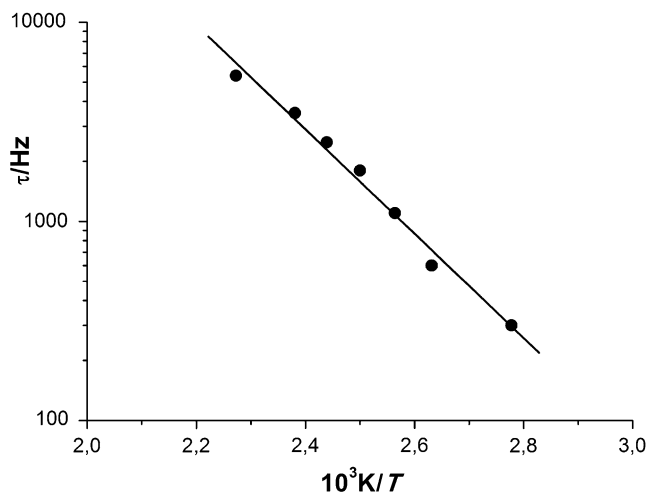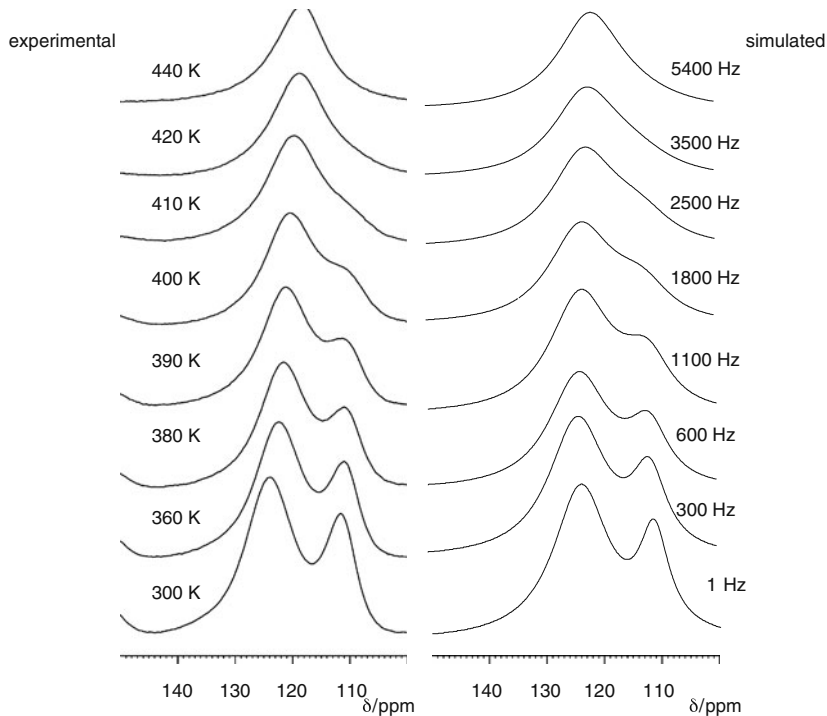

Fig. 6 Temperature dependence of the ^{7}Li exchange correlation frequencies ν. The slope of this Arrhenius plot corresponds to an activation energy of 50 kJ/mol

the rhombohedral symmetry. The Pt–Si distances within the Pt_9Si_2 units range from 238 to 246 pm, close to the sum of the covalent radii [19] of 246 pm. Similar Pt–Si distances also occur in the binary platinum silicides $Pt_{12}Si_5$ [20], Pt_2Si [21] and Pt_6Si_5 [22]. We can therefore assume substantial Pt–Si bonding within the $[Pt_3Si]$ network of Li_4Pt_3Si.

The trigonal $SiPt1_3Pt2_3$ prisms are capped by three lithium atoms on the rectangular sites, leading to coordination number 9. Such tricapped trigonal prisms are a typical geometrical motif in many intermetallic structure types [23,

Fig. 5 Experimental temperature-dependent ^{7}Li MAS NMR spectra of Li_4Pt_3Si and comparison with simulated spectra based on a two-site exchange model

24]. The edges of the trigonal prisms are quite short with Pt1–Pt2 distances of 274 pm, comparable to the Pt–Pt distance of 277 pm in *fcc* platinum [25]. Thus, the rigid three-dimensional [Pt$_3$Si] network (Fig. 2) is stabilised by Pt–Pt bonding as well.

The Li2–Si distances of 279 pm are significantly longer than the sum of the covalent radii of 240 pm [19]. Similar situation is observed in the binary lithium silicides [26]. The Li–Pt distances cover a broader range from 257 to 305 pm. The shorter ones compare well with the sum of the covalent radii of 252 pm [19] and with LiPt (264 pm) and Li$_2$Pt (276 pm) [27]. The coordination polyhedra of the two crystallographically independent lithium sites are presented in Fig. 3. Li1 and Li2 both have coordination number 13 with 6 Li+6 Pt+1 Si atom in their coordination shell. These two lithium species occur in a 3:1 ratio and with different site symmetry, i.e. (3.) for Li1 and (1) for Li2.

The lithium atoms as the less electronegative species in the Li$_4$Pt$_3$Si structure have most likely transferred part of their valence electrons to the more electronegative platinum and silicon atoms to enable the covalent bonding within the rigid [Pt$_3$Si] network. To a first approximation, we can write $(4Li)^{\delta+}[Pt_3Si]^{\delta-}$. The Li–Li distances range from 255 to 303 pm. The shorter Li–Li distances are all somewhat smaller than in *bcc* lithium (304 pm) [25], similar to the situation in LiRh$_2$Si$_2$ (275 pm) [28] and Li$_{13.7}$Rh$_8$Si$_{18.3}$ (268 pm) [9]. In view of the highly ionic character (and thus small size) of lithium in Li$_4$Pt$_3$Si (*vide infra*), these interactions may not be considered as bonding.

Summing up, the channels within the rigid [Pt$_3$Si] network of the Li$_4$Pt$_3$Si structure as well as the weaker bonding of the lithium to the platinum and silicon atoms are good structural prerequisites for lithium mobility (*vide infra*).

Solid-state NMR spectroscopy

Figure 4 shows the ^{7}Li MAS-NMR spectra of Li$_4$Pt$_3$Si at room temperature and at 470 K. At 300 K, the central $|1/2>$ $<->|-1/2>$ transition reveals two distinct signals at 112 and 123 ppm in a 3:1 ratio. Based on their intensity ratio, these signals can be assigned to Li(2) and Li(1), respectively, in excellent agreement with the structure solution. The large resonance shifts observed for both lithium sites reveal substantial Knight shift contributions, indicating that a significant amount of unpaired conduction electron density is localised at the ^{7}Li nuclei. Each resonance is flanked by a set of spinning sideband manifolds, attributed to the effect of MAS on the $|\pm1/2>$ $<->$ $|\pm3/2>$ satellite transitions, which are inhomogeneously broadened by the anisotropy of first-order quadrupolar perturbations. Note that this spinning sideband manifold extends over a much wider frequency range for the Li(2) species than for the Li(1) species, revealing a substantial difference in the local

electric field gradients. The smaller quadrupole splitting observed for the Li(1) species is consistent with the higher local symmetry of this site. The upper trace of Fig. 4 shows the spectrum at 470 K. Note that both resonances have collapsed into a single average signal, indicating fast lithium transfer between both sites on the relevant NMR timescale (the inverse difference between both resonance frequencies). Also, this spectrum reveals that lithium motion eliminates the spinning sideband manifolds arising from the first-order quadrupolar coupling effects, revealing that the corresponding ^{7}Li nuclei experience frequency changes owing to ionic hopping, which interfere with the ability of MAS to average out the inhomogeneous broadening effects during the rotor period. Figure 5 shows detailed temperature-dependent spectra and their simulations based on a simple two-site exchange model. For these simulations, only the central resonances were considered, and a constant line-broadening parameter was assumed. The correlation frequencies extracted from these simulations are plotted against inverse temperature. From the slope of this Arrhenius plot, we determine an activation energy of 50±1 kJ/mol, characterising the lithium transfer rate between both sites. These results demonstrate the dynamic character of the lithium ions in Li$_4$Pt$_3$Si and illustrate the ability of ^{7}Li solid-state NMR lineshape analyses to provide important quantitative information about their mobilities (Fig. 6).

References

1. Huggins RA (1999) Lithium alloys electrodes. In: Besenhard JO (ed) Handbook of battery materials, chapter 4. Wiley-VCH, Weinheim
2. Dimov N (2009) Development of metal alloy electrodes. In: Yoshio M, Brodd RJ, Kozawa A (eds) Lithium-ion batteries science and technology, chapter 11. Springer, Berlin, pp 241–265
3. Hoffmann R-D, Wu Zh, Pöttgen R (2003) Eur J Inorg Chem 3425
4. Wu Zh, Hoffmann R-D, Pöttgen R (2002) Z Anorg Allg Chem 628:1484
5. Wu Zh, Eckert H, Senker J, Johrendt D, Kotzyba G, Mosel BD, Trill H, Hoffmann R-D, Pöttgen R (2003) J Phys Chem B 107:1943
6. Sreeraj P, Wiemhöfer H-D, Hoffmann R-D, Skowronek R, Kirfel A, Pöttgen R (2006) J Solid State Chem 179:355
7. Sreeraj P, Kaskhedikar NA, Wiemhöfer H-D, Maier J, Pöttgen R (2010) Solid State Ionics 181:59
8. Pöttgen R, Wu Zh, Hoffmann R-D, Kotzyba G, Trill H, Senker J, Johrendt D, Mosel BD, Eckert H (2002) Heteroat Chem 13:506
9. Dinges T, Hoffmann R-D, Pöttgen R (2010) Z Naturforsch 65b:537

10. Dinges T, Hoffmann R-D, Pöttgen R (2008) Z Anorg Allg Chem 634:2034
11. Pöttgen R, Gulden Th, Simon A (1999) GIT Labor Fachz 43:133
12. Yvon K, Jeitschko W, Parthé E (1977) J Appl Crystallogr 10:73
13. Petricek V, Dusek M, Palatinus L (2006) Jana2006. The crystallographic computing system. Institute of Physics, Praha
14. Massiot D, Fayon F, Capron M, King I, Le Calvé S, Alonso B, Durand J-O, Bujoli B, Gan Z, Hoatson G (2002) Magn Reson Chem 40:70
15. Sheldrick GM (1997) SHELXS-97, program for the solution of crystal structures. University of Göttingen, Germany
16. Sheldrick GM (1997) SHELXL-97, program for crystal structure refinement. University of Göttingen, Germany
17. Flack HD, Bernadinelli G (1999) Acta Crystallogr 55A:908
18. Flack HD, Bernadinelli G (2000) J Appl Crystallogr 33:1143
19. Emsley J (1989) The Elements. Clarendon, Oxford
20. Gold W, Schubert K (1969) Z Kristallogr 128:406
21. Gohle R, Schubert K (1964) Z MetKd 55:503
22. Ram RP, Bhan S (1978) Z MetKd 69:524
23. Parthé E (1990) Elements of inorganic structural chemistry. Pöge, Leipzig
24. Parthé E, Gelato L, Chabot B, Penzo M, Cenzual K, Gladyshevskii R (1993) TYPIX—standardized data and crystal chemical characterization of inorganic structure types. Gmelin handbook of inorganic and organometallic chemistry, 8th edn. Springer, Berlin
25. Donohue J (1974) The structures of the elements. Wiley, New York
26. Nesper R (1990) Prog Solid State Chem 20:1
27. Bronger W, Nacken B, Ploog K (1975) J Less-Common Met 43:143
28. Dinges T, Rodewald UCh, Matar SF, Eckert H, Pöttgen R (2009) Z Anorg Allg Chem 635:1894